Increasing and widespread vulnerability of intact tropical rainforests to repeated droughts

Shengli Tao, Jérôme Chave, Pierre-Louis Frison, Thuy Le Toan, Philippe Ciais, Jingyun Fang, Wigneron J.-P., Maurizio Santoro, Hui Yang, Xiaojun Li, et al.

PNAS RESEARCH ARTICLE | ECOLOGY SUSTAINABILITY SCIENCE

Increasing and widespread vulnerability of intact tropical rainforests to repeated droughts

Shengli Tao[a,b,1], Jérôme Chave[a,1], Pierre-Louis Frison[c], Thuy Le Toan[d], Philippe Ciais[e], Jingyun Fang[b], Jean-Pierre Wigneron[f], Maurizio Santoro[g], Hui Yang[e], Xiaojun Li[f], Nicolas Labrière[a], and Sassan Saatchi[h]

Edited by Yadvinder Mahli, University of Oxford Environmental Change Institute, Oxford, United Kingdom; received September 13, 2021; accepted July 25, 2022 by Editorial Board Member Ruth DeFries

Intact tropical rainforests have been exposed to severe droughts in recent decades, which may threaten their integrity, their ability to sequester carbon, and their capacity to provide shelter for biodiversity. However, their response to droughts remains uncertain due to limited high-quality, long-term observations covering extensive areas. Here, we examined how the upper canopy of intact tropical rainforests has responded to drought events globally and during the past 3 decades. By developing a long pantropical time series (1992 to 2018) of monthly radar satellite observations, we show that repeated droughts caused a sustained decline in radar signal in 93%, 84%, and 88% of intact tropical rainforests in the Americas, Africa, and Asia, respectively. Sudden decreases in radar signal were detected around the 1997–1998, 2005, 2010, and 2015 droughts in tropical Americas; 1999–2000, 2004–2005, 2010–2011, and 2015 droughts in tropical Africa; and 1997–1998, 2006, and 2015 droughts in tropical Asia. Rainforests showed similar low resistance (the ability to maintain predrought condition when drought occurs) to severe droughts across continents, but American rainforests consistently showed the lowest resilience (the ability to return to predrought condition after the drought event). Moreover, while the resistance of intact tropical rainforests to drought is decreasing, albeit weakly in tropical Africa and Asia, forest resilience has not increased significantly. Our results therefore suggest the capacity of intact rainforests to withstand future droughts is limited. This has negative implications for climate change mitigation through forest-based climate solutions and the associated pledges made by countries under the Paris Agreement.

rainforests | drought | remote sensing | radar

Significance

Drought events affecting tropical rainforests are expected to become more frequent due to climate change. However, the ability of tropical rainforests to withstand drought remains controversial. We developed a radar data set that quantifies how global intact tropical rainforests have responded to droughts continuously since 1992. The radar instruments used in this study actively sense moisture levels of forest canopies, and they are insensitive to cloud cover. We found a long-term declining trend of radar signal in all three continents, and that most intact tropical rainforests have become increasingly vulnerable to drought. Thus, repeated droughts may navigate the world's last intact rainforests out of their normal functioning regime.

Global tropical rainforests absorb large amounts of carbon—an ecosystem service that offsets a large portion of the world's anthropogenic carbon emissions (1). Human activity is encroaching into tropical rainforests worldwide (2), making the service provided by the remaining intact tropical rainforests (i.e., those not affected by direct anthropogenic deforestation) increasingly valuable (3). However, intact tropical rainforests have suffered frequent droughts in recent decades (4–7). How have intact tropical rainforests responded to droughts in the past? Will they be able to buffer future droughts? The answers to these two questions remain uncertain, since some studies have reported strong drought resistance (8, 9), while others predict drought-induced tropical forest dieback (10).

A major reason for this uncertainty is the scarcity of long-term and spatially extensive monitoring of tropical rainforests. Long-term observation is important because the impact of repeated droughts cannot be easily inferred from the short-term impact of individual droughts (11). Studies of a few severe drought events (4–8, 12–14) do not highlight the long-term response of tropical rainforests, which is crucial for predicting the forest response to future droughts. Extensive spatial coverage is needed as local studies have given conflicting results (15–17).

One long-term global data set that can provide indications on the response of intact tropical rainforests to drought is represented by the "greenness" of vegetation derived from optical remote sensing observations. However, interpretation of tropical rainforest greenness trends may lead to misleading conclusions due to issues such as cloud contamination (8, 18–20). Microwave signals acquired during all weather conditions overcome the problem of pervasive cloudiness over wet tropical forests. As such, microwave signals have the potential to provide a significant advance in the understanding of drought effects on tropical rainforests.

Microwave signals acquired by either passive (radiometer) or active (radar) sensors are sensitive to forest water content (total mass of water in aerial living tissues), which is related to forest dry biomass and tissue moisture (mass of water per unit mass of dry

Author contributions: S.T. and J.C. designed research; S.T. and J.C. performed research; S.T., J.C., P.-L.F., T.L.T., P.C., J.F., J.P.W., M.S., H.Y., X.L., N.L., and S.S. analyzed data; S.T., J.C., P.L.F., T.L.T., P.C., J.F., J.P.W., M.S., H.Y., X.L., N.L., and S.S. wrote the paper; and all authors interpreted the results and edited the text.

The authors declare no competing interest.

This article is a PNAS Direct Submission. Y.M. is a guest editor invited by the Editorial Board.

[1]To whom correspondence may be addressed. Email: sltao@pku.edu.cn or jerome.chave@univ-tlse3.fr.

This article contains supporting information online at http://www.pnas.org/lookup/suppl/doi:10.1073/pnas.2116626119/-/DCSupplemental.

Published September 6, 2022.

biomass) (21). In addition, microwave signals penetrate clouds and rain over rainforests with negligible attenuation—if the wavelength is much larger than the size of raindrops, for example, at ∼6 cm, also called the C radiofrequency band (*SI Appendix*, Fig. S1). However, there is not a single microwave data set acquired at C-band or longer wavelength that spans more than 2 decades (22–24; *SI Appendix*), which limits the use of these data for the trend analysis of forest response to drought. We have created a harmonized pantropical C-band radar data set at 25 km resolution from 1992 to 2018 (*SI Appendix*, Figs. S2 and S3). This time series can in principle be extended beyond 2018 as similar C-band radar missions are secured in the forthcoming decades. In closed forest environments, the C-band radar signal penetrates a few meters into the canopy (25), and thus mainly measures the dynamics of the upper canopy. Temporal fluctuations in the C-band radar signal are due to seasonal changes in canopy moisture and long-term changes in canopy structure, both of which quantify the response of forests to environmental factors, such as drought (21).

We analyzed the correlation between the radar backscattered intensity signal (expressed in decibels [dB]; *Materials and Methods*) and all of the drought events since 1992. This study was restricted to intact tropical rainforests, formally defined as pixels with less than 5% cumulative forest degradation or deforestation throughout the study period, to avoid confounding effects of land-cover change (2) (*Materials and Methods*). We explored the long-term trends in radar signal, and the changes in vulnerability of rainforests to repeated droughts. Droughts were detected using the cumulative water deficit (CWD, negative values signifying water stress), which is robust to site-level studies (6, 26). The CWD index was calculated as the cumulative monthly deficit of precipitation (27) minus evapotranspiration (*SI Appendix*, Fig. S4; 28).

RESULTS

Drought Responses of Intact Tropical Rainforests across Continents. In the American tropics, the radar signal declined continuously during the study period at a rate of $-4.8\ 10^{-3}$ dB y^{-1} ($P < 0.001$; Fig. 1*A*). Sudden decreases, or "breaks," in radar signal were detected (*Materials and Methods*), corresponding to the droughts of 1997–1998, 2005, 2010, and 2015 (*SI Appendix*, Fig. S5*A*). In tropical Africa, a long-term and significant decline in the radar signal was also observed ($-2.7\ 10^{-3}$ dB y^{-1}, $P < 0.001$; Fig. 1*B*). Breaks in the radar signal were detected during the droughts of 1999–2000, 2004–2005, 2010–2011, and 2015 (*SI Appendix*, Fig. S5*B*). The 2004–2005 African drought, although not the most severe, was followed by continued water stress in 2006 and 2007 (Fig. 1*B*; 29), which disrupted the trend of increasing radar signal before 2004 and caused a sudden decline thereafter (*SI Appendix*, Fig. S5*B*).

A long-term decreasing trend in the radar signal of $-4.3\ 10^{-3}$ dB y^{-1} ($P < 0.001$) was also detected in tropical Asia (Fig. 1*C*). Breaks in the radar signal were detected around the 1997–1998, 2006, and 2015–2016 Asian droughts (*SI Appendix*, Fig. S5*C*). The impacts of the mega-droughts associated with the extreme El Niño events of 1997–1998 and 2015–2016 were the most pronounced (Fig. 1*C*). However, the radar signal decreased significantly even when both mega-droughts were ignored. Also, the recovery trajectories after these two droughts differed, the former causing a break in the radar signal that was not recovered until 2018, whereas the latter was followed by a rapid postdrought recovery (Fig. 1*C* and *SI Appendix*, Fig. S5*C*). Compared to the African and American tropics, the seasonality of the radar signal was the weakest in Asia, likely due to the weak seasonality of precipitation in tropical Asia.

These trends do not coincide with changes in radar sensors, and are therefore unlikely to be due to an instrumental artifact (*SI Appendix*). The trends were also tested against the influence of spatial autocorrelation in the radar signal. Toward this purpose, we selected pixels that have low signal correlations (Pearson $r < 0.5$). Similar declining trends (Pearson $r \geq 0.92$) were still observed, suggesting the robustness of the trends against spatial autocorrelation (*SI Appendix*, Fig. S6).

Spatial Patterns of the Trend in Radar Signal. In the American tropics, 93% of the intact rainforest pixels (∼2.3 million km^2 in total, with each pixel 25 × 25 km) showed decreasing trends in radar signal, with south and southwest of Amazonia decreasing the most (Fig. 2*A*). In Africa, 84% (0.6 million km^2) of intact rainforests showed a decline in the radar signal, but 18% of the pixels had the opposite trend (Fig. 2*B*). In Asia, the trend of decrease in the radar signal was also widespread, occurring in 88% (0.28 million km^2) of all intact rainforests. We verified that the upward or downward trends in the signal were not due to different deforestation/degradation intensities, but to different water stress legacies, suggesting that water stress is the primary driver of the radar signal trends (*SI Appendix*, Fig. S7). We also found that the radar signal correlated not only with the CWD index (median Pearson $r = 0.44$) but also with land surface temperature (median Pearson $r = -0.47$) and air temperature (median Pearson $r = -0.50$), two other proxies of climate anomaly (*SI Appendix*, Fig. S8; 30, 31). In ever-wet forests, without a pronounced dry season, such as in northwest Amazonia,

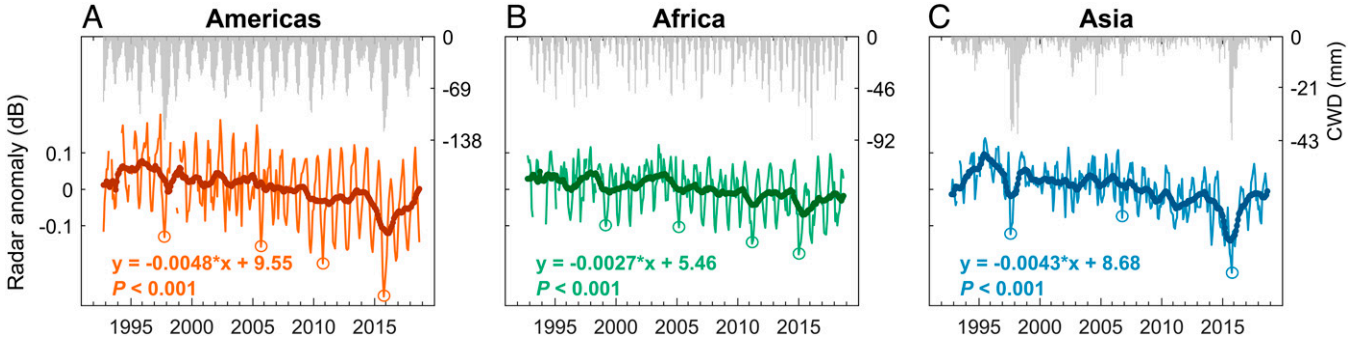

Fig. 1. Drought response of intact tropical rainforests, 1992 to 2018. Monthly radar signal anomaly and CWD at the continental level (average across all pixels) were shown for intact tropical rainforests in (*A*) the Americas, (*B*) Africa, and (*C*) Asia. In each panel, radar signal anomaly was calculated as a deviation from the long-term average value and represented by a thin line, and the 12-mo moving average of the signal was shown as a thick line. A linear regression was fitted to the monthly radar signal and the regression equation is presented in the lower-left corner of each subset. Drought events that caused "breaks" in radar signal are marked by circles (see *SI Appendix*, Fig. S5 for the detection of the "breaks").

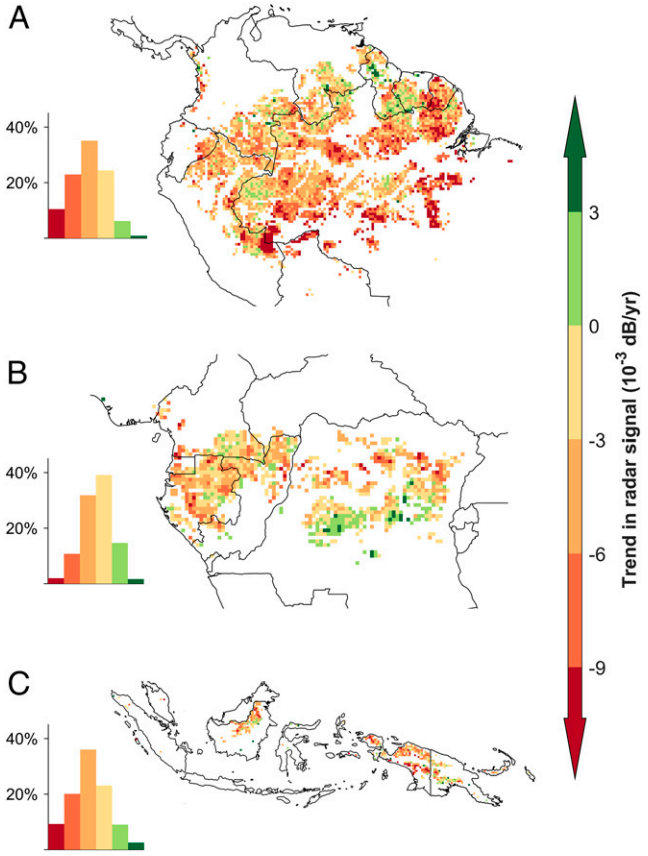

Fig. 2. Spatial patterns of the radar signal trends (1992–2018) for the (*A*) American, (*B*) African, and (*C*) Asian intact tropical rainforests. A linear regression was fitted to the monthly radar signals in each intact tropical rainforest pixel, and the slope of the regression is reported. The histograms beside each regional map show the proportion of pixels in each trend class. The color bar and numeric legend values are the same in the histograms and maps.

CWD values were usually close to zero, generating a weak and nonsignificant correlation ($P > 0.05$, *SI Appendix*, Fig. S8 *A* and *B*). However, rare events of water deficit were observed in ever-wet forests, and during these periods the radar signal decreased as expected (*SI Appendix*, Fig. S9). These results show that the long-term decline of the radar signal reflects the legacy effect of droughts on forest canopy structure across intact tropical rainforests.

Rainforest Resistance and Resilience to Drought Events. We then explored the drought resistance and resilience of intact rainforests. To identify past droughts, we calculated maximum CWD (MCWD) for each year and each pixel (4, 5, 26). The Z score of MCWD was then calculated, and droughts were defined as years with a Z score value below -1. To aid the interpretation of figures, drought severity was then calculated as the absolute value of the Z score of MCWD. For each drought event, drought resistance was defined as the relative rate of change in forest condition during and before drought disturbance and drought resilience as the ability to recover to the pre-drought state (32–34). We studied resistance and resilience 2 years before and 2 years after the drought event; this time span accounts for the 2-year legacy effect of drought previously reported in rainforests (35). Although some rainforests need a longer time to recover, the rate of recovery after a fixed period of time is already an indication of the forest's ability to recover from droughts. The pixel-level results were summarized at the continental scale by taking the median value of all pixels (Figs. 3 and 4). We verified that our conclusions were not altered if a longer drought legacy window (i.e., 3 instead of 2 years), a constant evapotranspiration of 100 mm/mo for calculating MCWD (26), a more severe water stress threshold for defining past droughts (i.e., -1.5 rather than -1), and detrended radar signals were used (*SI Appendix*, Figs. S10–S13). We also verified that the conclusions were not altered when the self-calibrating Palmer Drought Severity Index (scPDSI) was used instead of the Z score of MCWD to identify past drought events (*SI Appendix*, Fig. S14; 36).

We found that the radar signal decreased with increasing drought severity in all three continents (Fig. 3 *A*–*C*), suggesting that intact tropical rainforests are generally vulnerable to severe droughts. The decreasing trend of resistance with increasing drought severity was most pronounced and significant in the tropical Americas (Fig. 3*A*). With respect to drought resilience, American rainforests did not recover to predrought conditions after droughts with a severity (i.e., the absolute value of the Z score of MCWD) >1.5 (Fig. 3*D*). In contrast, African and Asian rainforests were resilient to severe droughts with a severity >2 (Fig. 3 *E* and *F*). This could be due to the higher frequency of droughts in Africa and Asia historically (29).

The above results also suggest the existence of a threshold of drought impact beyond which forest resilience was systematically negative, implying the risk of a forest dieback. We explored further the existence of this threshold. We found that, in the Americas, 50% of the intact tropical rainforest pixels did not return to predrought conditions when drought severity exceeded a pixel-specific threshold. This threshold was defined as the drought severity value beyond which resilience was always negative in the pixel. This fraction was also detectable but lower in Africa (43%) and in Asia (27%; *SI Appendix*, Fig. S15). These results show that on a global scale, intact tropical rainforests are not resistant to severe droughts. Also, American intact rainforests are most vulnerable to severe droughts because of their poor ability to recover to predrought conditions.

Temporal Trends in Rainforest Resistance and Resilience. Finally, we explored how drought resistance and resilience have changed during the last 3 decades. We found a decrease in drought resistance in all three continents, with the strengths of trends varying from -0.19 to -0.41 (τ value of the Mann-Kendall test; $\tau = -1$ indicates a strong decrease, while $\tau = 1$ indicates a strong increase) (Fig. 4). The most pronounced trend of decreasing resistance was found in the American tropics ($\tau = -0.41$; two-tailed $P < 0.05$). At the same time, resilience did not increase significantly on a global scale: it decreased in the Americas ($\tau = -0.29$) and did not change significantly in the African and Asian tropics ($|\tau| \leq 0.07$; $P > 0.05$). Pixel-level analyses were consistent with regional results: the median value of the trends in resistance across pixels was the lowest in the Americas (-0.5), followed by Asia (-0.48) and Africa (-0.4), while the median of the trends in resilience was slightly negative or close to zero (*SI Appendix*, Fig. S16). Thus, on a global scale, the majority of intact tropical rainforests appears to be increasingly vulnerable to drought, with decreasing resistance but no obvious increase in resilience. This is especially the case in the tropical Americas.

DISCUSSION

Interpreting the Long-Term Declines in Radar Signal. We quantified the long-term vulnerability of intact rainforests to repeated droughts, detected by persistent trends of declining

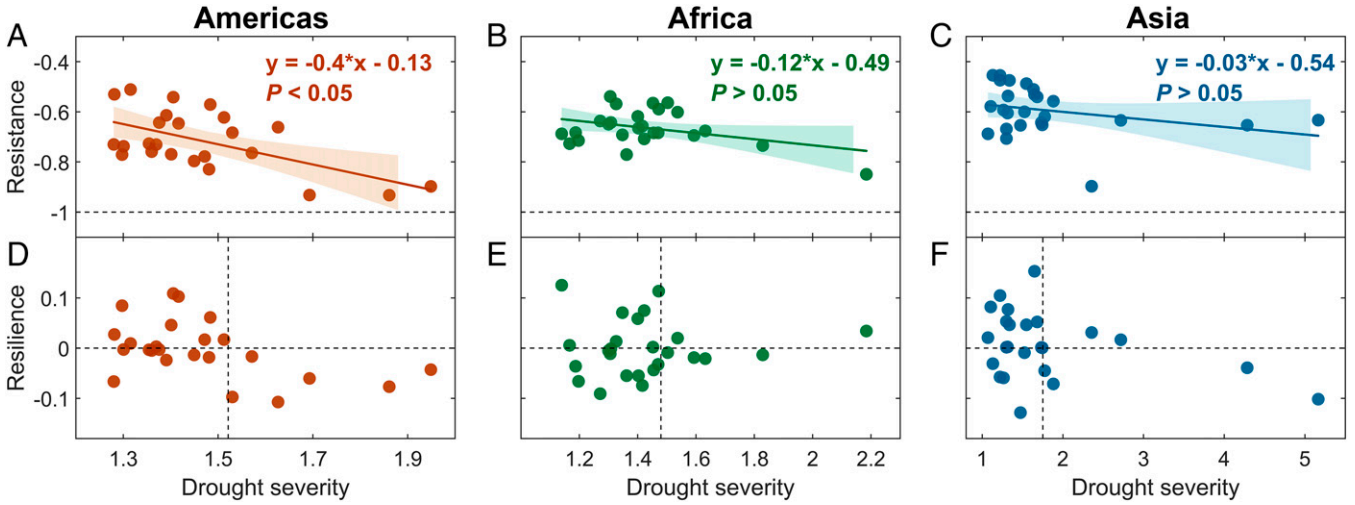

Fig. 3. Drought resistance and resilience versus drought severity in intact tropical rainforests in the Americas, Africa, and Asia. For each drought event, the median resistance, resilience, and drought severity of the drought-affected pixels (*Z* score of MCWD <−1) were calculated. The drought severity was defined as the absolute value of the *Z* score of MCWD. Resistance was computed so that lower values mean a more severe decrease in radar signal during a drought. A resistance of zero means no decrease in radar signal during the drought, and −1 is the minimum value for resistance (dashed lines in *A*–*C*). A trend fitting was performed in *A*–*C*, with its equation labeled and 95% confidence bound shaded. Regarding resilience (*D*–*F*), a positive value means that the forest recovered to predrought conditions, while a negative value means that it did not (for pixel-level analyses, see *SI Appendix*, Fig. S15). In *D*–*F*, a horizontal dashed line was drawn to indicate the resilience value of zero, and a vertical dashed line drawn at the 75th percentile of all drought severities.

radar signal in tropical canopies in nearly 3 decades. Several hypotheses can be proposed to explain the observed long-term trends in radar signal (*SI Appendix*, Sections 12–17).

The declines do not appear to be related to the processing of the radar data (*SI Appendix*, Figs. S2 and S3), to data acquisition time or polarization mode (*SI Appendix*, Fig. S17), or to filtering due to heavy rain events (*SI Appendix*, Fig. S18). We verified that these declines were not caused by direct anthropogenic effects since nonforested areas and degraded or deforested pixels were conservatively masked (*SI Appendix*, Figs. S7 and S19). Two additional forest masks were tested, and similar radar signal trends were obtained (*SI Appendix*, Fig. S20). We also verified that recent increases in dry season length in southern Amazonia (37) and Africa (38) were not responsible for the decreasing trends in the radar signal (*SI Appendix*, Fig. S21).

Soil moisture has recently been found to influence the vegetation optical depth retrieved from passive microwave signals (39). However, in contrast to passive microwave sensors (12, 22–24), the radar instruments used here actively emit a microwave and measure the intensity of backscattered waves. Given the dense canopy of the intact rainforest and the shallow penetration depth of the C-band signal (up to a few meters, 25), the radar backscatter was found to be little influenced by soil moisture (*SI Appendix*, Fig. S22).

Leaf water (both surface and internal water content) has been reported to influence microwave signals, but mostly at the diurnal time scale (40, 41). However, here, we observed sustained radar signal declines extending nearly 3 decades, and these declines do not match the long-term changes in either leaf surface water or leaf internal water (*SI Appendix*, Figs. S23 and S24). Thus, leaf water dynamic is not responsible for the long-term declining radar signal trends.

Radar Signal and Biomass Changes. Since the observed long-term decrease in radar signal cannot be explained by deforestation or forest degradation, or by trends in leaf and soil moisture, we hypothesize that variations in radar signal reflect the forest top-canopy dynamics and are therefore expected to correlate

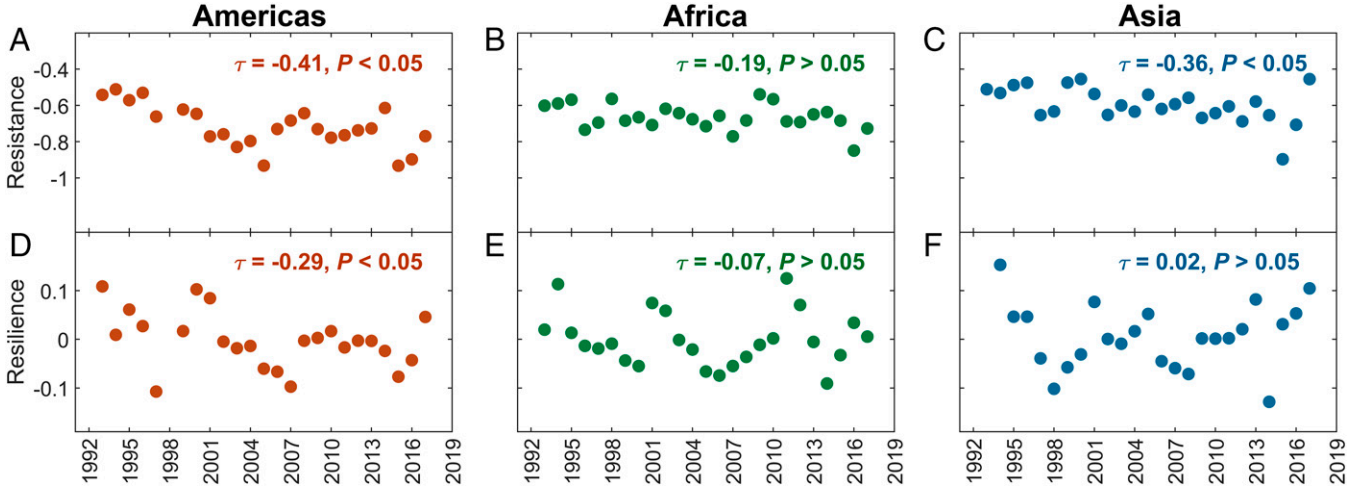

Fig. 4. Time series of drought resistance and resilience of intact tropical rainforests in (*A* and *D*) the Americas, *(B* and *E)* Africa, and *(C* and *F*) Asia. Resistance and resilience were calculated as in Fig. 3, but presented by year to assess their temporal trends. The direction and strength of the trend were evaluated by the Mann-Kendall τ value, labeled in each subset, and significance was assessed by a two-tailed *P* value (for pixel-level analyses, see *SI Appendix*, Fig. S16).

with changes in forest biomass, due to, for example, drought-induced defoliation, branch fall, or tree mortality (35, 42, 43). To test this hypothesis, we compared the radar signals with two products of forest carbon changes (22, 44) and obtained similarly declining trends (Pearson $r \geq 0.84$; *SI Appendix*, Fig. S25).

We also compared radar signal changes during the 2005 and 2010 drought events to the only Amazonian forest plot data available to explore the response of tropical forest biomass to megadroughts (6, 13). We found that the intensity of radar signal decline during droughts correlated significantly with plot biomass declines ($P < 0.05$; *SI Appendix*, Fig. S26), despite the scale mismatch between plot (~1 ha) and radar pixel (25 km), and hence the strength of the correlation. These analyses support the hypothesis that the radar signal used in this study detect drought-induced forest biomass loss. Thus, the long-term declines in radar signal can be in part interpreted as being due to a decline in forest biomass, because repeated droughts result in an overall reduction in forest productivity, an increase in mortality, or a combination of both as shown by ground observations (6, 13, 35). Our results are therefore consistent with a previous report of a recent decline in tropical forest carbon sink intensity (45).

Implications for Rainforest Conservation. Our analyses suggest a decrease in drought resistance of intact rainforests but no significant increase in resilience (Figs. 3 and 4), implying an increasing vulnerability of intact tropical rainforests. A recent study has shown that tropical forest biomass is increasingly vulnerable to climate and human stressors, but especially in deforested regions (46), and it again highlights the difficulty of assessing the climate vulnerability of intact tropical rainforests due to data scarcity. By developing a long-term radar observation validated as suitable for trend analysis (*SI Appendix*, Fig. S3), we report a widespread increasing vulnerability of global intact tropical rainforests to one of the most important climate stressors, drought. Our results are therefore of major importance as modeled climate scenarios of the 21st century indicate an increase in drought frequency and air temperature in the tropics (47). Intact tropical rainforests are a key component of the natural climate solution for mitigating climate change (48). However, our results call into question the ability of intact tropical rainforests, particularly in the American tropics, to withstand future droughts and persist as atmospheric carbon sinks. Tropical forest dieback could lead to further losses of carbon to the atmosphere, which would undermine the goal of the Paris Agreement of keeping global warming well below 2 °C, with disastrous consequences for biodiversity and the hydrological cycle.

Materials and Methods

We examined satellite microwave data from the C-band (~6 cm wavelength) radar scatterometers ERS-1/-2 (1992 to 2001) and ASCAT (2007 to 2018). C-band signals are unaffected by the dense cloud cover over tropical rainforests. ASCAT is still in operation, making it possible to monitor future droughts. The radar backscatter is usually expressed in decibels, the logarithmic of the ratio of received over emitted signals. A small change in radar signal can reflect a shift in forest condition (*SI Appendix*, Fig. S1): the median value of the radar signal is −7.8 dB over evergreen tropical rainforests, only 1.1 dB higher than that of deciduous forests (−8.9 dB). The 7-year data gap between ERS and ASCAT was filled with data from the Ku-band QSCAT scatterometer (~2 cm wavelength, 1999 to 2009). Backscatter values from the different sensors were first scaled against the ASCAT baseline (*SI Appendix*, Fig. S27). For each pixel, a model was then built to predict the monthly signal differences between Ku-band and C-band signals in the overlapping years (1999 to 2001 and 2007 to 2009), using rainfall amount as a predictor (*SI Appendix*, Figs. S28 and S29). The predictive models had an overall median r value of 0.64, suggesting relatively high accuracy. For each pixel, the model was then applied on the entire QSCAT time series from 1999 to 2009. There remain some differences between the corrected Ku-band and C-band monthly signals (*SI Appendix*, Fig. S30), but the gap-filled radar signal did not display detectable bias. As shown in *SI Appendix*, Fig. S3, we compared the gap-filled signals against C-band ERS observations that were continuously available until 2011 for a subset of pixels (49), and obtained r values of 0.92 and 0.88 in tropical American and Asian rainforests, respectively.

To avoid confounding effects of forest degradation or deforestation, we restricted this analysis to intact tropical rainforests. A 25-km radar pixel was classified as intact tropical rainforest if at least 95% of the pixel area was never disturbed or deforested between 1992 and 2018, according to a high-resolution (30 m) land cover change map (2). This selection resulted in a data set of ca. 3,800, 1,100, and 430 radar pixels for the tropical Americas, Africa, and Asia, respectively. We verified that the radar signal trends were not caused by the choice of the 5% threshold, using three approaches detailed in *SI Appendix*, Section 12. We also verified that the spatially averaged radar signal trends shown in Fig. 1 are robust to spatial autocorrelation in the radar signal (*SI Appendix*, Fig. S6).

We used the BFAST (Breaks for Additive Season and Trend) algorithm to explore whether past droughts have caused sudden decreases (or, "breaks") in radar signal (*SI Appendix*, Fig. S5). BFAST detects discontinuities in a time series by fitting piecewise linear models iteratively to different sections of the time series (50). We set the parameter "*h*" of BFAST (minimal length between potential breaks, given as fraction relative to the total length) at 0.15 (the default value), and the parameter "*breaks*" (maximum number of potential breaks to be detected) at 5, based on the fact that severe droughts occurred in tropics every ca. 5 y.

To study the drought resistance and resilience of rainforests, drought events were first identified using the standardized anomaly (or *Z* score) of maximum cumulative water deficit within 1 year (MCWD), calculated from the Climate Hazards Group InfraRed Precipitation with Station rainfall data (27) and Global Land *Evaporation* Amsterdam Model evapotranspiration data (version 3.3a, *SI Appendix*, Fig. S4; 28). A threshold of −1 was applied on the *Z* score of MCWD to identify past drought events. Drought severity was then taken to be the absolute value of the *Z* score of MCWD. Drought resistance and resilience were calculated following standard definitions in the ecological literature (32–34). Defining Y_{pre} as the predrought radar signal, Y_{post} as the signal postdrought, and Y_e as the signal during the drought event, resistance was defined as $(Y_e - Y_{pre})/Y_{pre}$, and resilience as $(Y_{post} - Y_{pre})/Y_{pre}$ (34). We used the maximum radar (wet season) signal values within 2 years before and 2 years after the drought event to represent forest pre- and postdrought conditions, respectively. We used radar maxima to ensure that the forest conditions before and after the drought have comparable moisture levels. Resilience is therefore expected to reflect changes in forests structure due to canopy disturbance more than changes in moisture (21). The use of a 2-year time window accounts for the 2-year legacy effect of drought previously reported in rainforests (35). Resistance and resilience were calculated for each pixel and for all of the drought events during the past 3 decades, and were reported at the continental scale by taking the median value across drought-affected pixels (Figs. 3 and 4). We tested whether more severe droughts caused a more intense decrease in radar signal (or, lower resistance; Fig. 3). To test the increasing vulnerability of rainforests to droughts, we quantified the temporal changes in resistance/resilience using the Mann-Kendall τ (or, tau) test (Fig. 4).

We then verified the robustness of the conclusions drawn from Figs. 3 and 4. Specifically, we tested a longer drought legacy window (i.e., 3 rather than 2 years), a lower threshold for *Z* score of MCWD (i.e., −1.5 rather than −1), detrended radar signals, a constant evapotranspiration of 100 mm/mo in the calculation of MCWD (26), and a different drought index for defining past droughts, namely the Climatic Research Unit (CRU) scPDSI (36). The results of these sensitivity tests are shown in *SI Appendix*, Figs. S10–S14.

Finally, we explored the long-term declines in radar signal against soil moisture (*SI Appendix*, Fig. S22), forest degradation or deforestation intensity (*SI Appendix*, Figs. S7, S19, and S20), data acquisition time or polarization mode (*SI Appendix*, Fig. S17), heavy rain events (*SI Appendix*, Fig. S18), dry season length (*SI Appendix*, Fig. S21), leaf surface water (*SI Appendix*, Figs. S23 and S24), and forest biomass (*SI Appendix*, Figs. S25 and S26). In particular, radar signal changes were compared with two time series of forest biomass products

(22, 44; *SI Appendix*, Fig. S25), and further with plot biomass changes for two major drought events occurring in Amazonia (i.e., the 2005 and 2010 droughts; 6, 13; *SI Appendix*, Fig. S26). More details about the data and methods can be found in the *SI Appendix*.

Data, Materials, and Software Availability. Radar images were provided by EUMETSAT (https://navigator.eumetsat.int/search?query=&filter=themes__Land) and BYU (Brigham Young University) Data Center (https://www.scp.byu.edu/). Codes and processed radar images in the formats of 'mat' and 'nc' are publicly available at https://github.com/TonySl/Radar_Rainforest and https://doi.org/10.6084/m9.figshare.14061428.v6.

ACKNOWLEDGMENTS. We gratefully acknowledge help and discussions with the following colleagues: A. G. Dai, T. R. Feldpausch, Y. Jiang, O. L. Phillips, C. Chen, L. Xu, Y. Yang, and L. M. Zhou. We warmly thank the three anonymous reviewers for their insightful comments. This study was supported by an Investissement d'Avenir grant managed by the Agence Nationale de la Recherche (CEBA, ref. ANR-10-LABX-25-01; TULIP, ref. ANR-10-LABX-0041; ANAEE-France: ANR-11-INBS-0001), and by the National Natural Science Foundation of China (grant no. 31988102). This research was also supported by a Centre National d' Etudes Spatiales (CNES) postdoctoral fellowship to S.T., the CNES-BIOMASS pluriannual project, and the European Space Agency (ESA) Climate Change Initiative (CCI) Biomass project (contract no. 4000123662/18/I-NB). P.C. acknowledges supports from the ESA CCI RECCAP2 project (ESRIN/4000123002/18/I-NB).

Author affiliations: [a]Laboratoire Évolution et Diversité Biologique, UMR 5174 (CNRS/IRD/UPS), 31062 Toulouse Cedex 9, France; [b]Institute of Ecology, College of Urban and Environmental Sciences, and Key Laboratory for Earth Surface Processes of the Ministry of Education, Peking University, Beijing 100871, China; [c]LaSTIG, Université Gustave Eiffel, ENSG, IGN, F-77420 Champs-sur-Marne, France; [d]Centre d'Etudes Spatiales de la Biosphère, CNRS-CNES-UPS-IRD, 31400 Toulouse, France; [e]Laboratoire des Sciences du Climat et de l'Environnement/IPSL, CEA-CNRS-UVSQ, Université Paris Saclay, 91191 Gif-sur-Yvette, France; [f]ISPA, UMR 1391, INRAE Nouvelle-Aquitaine, Université de Bordeaux, Grande Ferrade, Villenave d'Ornon, 33140 France; [g]Gamma Remote Sensing, 3073 Gümligen, Switzerland; and [h]Jet Propulsion Laboratory, California Institute of Technology, Pasadena, CA 91109

1. Y. Pan *et al.*, A large and persistent carbon sink in the world's forests. *Science* **333**, 988–993 (2011).
2. C. Vancutsem *et al.*, Long-term (1990–2019) monitoring of forest cover changes in the humid tropics. *Sci. Adv.* **7**, eabe1603 (2021).
3. A. M. Osuri *et al.*, Greater stability of carbon capture in species-rich natural forests compared to species-poor plantations. *Environ. Res. Lett.* **15**, 034011 (2020).
4. S. Saatchi *et al.*, Persistent effects of a severe drought on Amazonian forest canopy. *Proc. Natl. Acad. Sci. U.S.A.* **110**, 565–570 (2013).
5. S. L. Lewis, P. M. Brando, O. L. Phillips, G. M. van der Heijden, D. Nepstad, The 2010 Amazon drought. *Science* **331**, 554 (2011).
6. O. L. Phillips *et al.*, Drought sensitivity of the Amazon rainforest. *Science* **323**, 1344–1347 (2009).
7. J. C. Jiménez-Muñoz *et al.*, Record-breaking warming and extreme drought in the Amazon rainforest during the course of El Niño 2015-2016. *Sci. Rep.* **6**, 33130 (2016).
8. S. R. Saleska, K. Didan, A. R. Huete, H. R. da Rocha, Amazon forests green-up during 2005 drought. *Science* **318**, 612–612 (2007).
9. C. Huntingford *et al.*, Simulated resilience of tropical rainforests to CO_2-induced climate change. *Nat. Geosci.* **6**, 268–273 (2013).
10. Y. Malhi *et al.*, Exploring the likelihood and mechanism of a climate-change-induced dieback of the Amazon rainforest. *Proc. Natl. Acad. Sci. U.S.A.* **106**, 20610–20615 (2009).
11. P. Meir *et al.*, Short-term effects of drought on tropical forest do not fully predict impacts of repeated or long-term drought: Gas exchange versus growth. *Philos. Trans. R. Soc. Lond. B Biol. Sci.* **373**, 20170311 (2018).
12. J. P. Wigneron *et al.*, Tropical forests did not recover from the strong 2015-2016 El Niño event. *Sci. Adv.* **6**, eaay4603 (2020).
13. T. R. Feldpausch *et al.*, Amazon forest response to repeated droughts. *Global Biogeochem. Cycles* **30**, 964–982 (2016).
14. W. R. Anderegg, A. T. Trugman, G. Badgley, A. G. Konings, J. Shaw, Divergent forest sensitivity to repeated extreme droughts. *Nat. Clim. Chang.* **10**, 1091–1095 (2020).
15. D. Zuleta, A. Duque, D. Cardenas, H. C. Muller-Landau, S. J. Davies, Drought-induced mortality patterns and rapid biomass recovery in a terra firme forest in the Colombian Amazon. *Ecology* **98**, 2538–2546 (2017).
16. P. R. L. Bittencourt *et al.*, Amazonian trees have limited capacity to acclimate plant hydraulic properties in response to long-term drought. *Glob. Change Biol.* **26**, 3569–3584 (2020).
17. C. E. Doughty *et al.*, Drought impact on forest carbon dynamics and fluxes in Amazonia. *Nature* **519**, 78–82 (2015).
18. D. C. Morton *et al.*, Amazon forests maintain consistent canopy structure and greenness during the dry season. *Nature* **506**, 221–224 (2014).
19. L. O. Anderson *et al.*, Vulnerability of Amazonian forests to repeated droughts. *Philos. Trans. R. Soc. Lond. B Biol. Sci.* **373**, 20170411 (2018).
20. G. P. Asner, A. Alencar, Drought impacts on the Amazon forest: The remote sensing perspective. *New Phytol.* **187**, 569–578 (2010).
21. A. G. Konings, K. Rao, S. C. Steele-Dunne, Macro to micro: Microwave remote sensing of plant water content for physiology and ecology. *New Phytol.* **223**, 1166–1172 (2019).
22. Y. Y. Liu *et al.*, Recent reversal in loss of global terrestrial biomass. *Nat. Clim. Chang.* **5**, 470–474 (2015).
23. L. Moesinger *et al.*, The global long-term microwave Vegetation Optical Depth Climate Archive (VODCA). *Earth Syst. Sci. Data* **12**, 177–177 (2020).
24. J. Du *et al.*, A global satellite environmental data record derived from AMSR-E and AMSR2 microwave earth observations. *Earth Syst. Sci. Data Discuss.* **9**, 791–808 (2017).
25. C. C. Carabajal, D. J. Harding, SRTM C-band and ICESat laser altimetry elevation comparisons as a function of tree cover and relief. *Photogramm. Eng. Remote Sensing* **72**, 287–298 (2006).
26. L. E. O. Aragão *et al.*, Spatial patterns and fire response of recent Amazonian droughts. *Geophys. Res. Lett.* **34**, L07701 (2007).
27. C. Funk *et al.*, The climate hazards infrared precipitation with stations–a new environmental record for monitoring extremes. *Sci. Data* **2**, 150066 (2015).
28. B. Martens *et al.*, GLEAM v3: Satellite-based land evaporation and root-zone soil moisture. *Geosci. Model Dev.* **10**, 1903–1925 (2017).
29. S. Asefi-Najafabady, S. Saatchi, Response of African humid tropical forests to recent rainfall anomalies. *Philos. Trans. R. Soc. Lond. B Biol. Sci.* **368**, 20120306 (2013).
30. Z. Wan, New refinements and validation of the MODIS land-surface temperature/emissivity products. *Remote Sens. Environ.* **112**, 59–74 (2008).
31. J. Muñoz Sabater, ERA5-land monthly averaged data from 1950 to 1980. Copernicus Climate Change Service (C3S) Climate Data Store (CDS) (2021). https://cds.climate.copernicus.eu/cdsapp#!/dataset/reanalysis-era5-land-monthly-means?tab=overview. Accessed 11 November 2021.
32. C. W. MacGillivray *et al.*, Testing predictions of resistance and resilience of vegetation subjected to extreme events. *Funct. Ecol.* **9**, 640–649 (1995).
33. D. Tilman, J. A. Downing, Biodiversity and stability in grasslands. *Nature* **367**, 363–365 (1994).
34. F. Lloret, E. G. Keeling, A. Sala, Components of tree resilience: Effects of successive low-growth episodes in old ponderosa pine forests. *Oikos* **120**, 1909–1920 (2011).
35. O. L. Phillips *et al.*, Drought-mortality relationships for tropical forests. *New Phytol.* **187**, 631–646 (2010).
36. G. van der Schrier, J. Barichivich, K. R. Briffa, P. D. Jones, A scPDSI-based global data set of dry and wet spells for 1901-2009. *J. Geophys. Res. Atmos.* **118**, 4025–4048 10.1002/jgrd.50355. (2013).
37. R. Fu *et al.*, Increased dry-season length over southern Amazonia in recent decades and its implication for future climate projection. *Proc. Natl. Acad. Sci. U.S.A.* **110**, 18110–18115 (2013).
38. Y. Jiang *et al.*, Widespread increase of boreal summer dry season length over the Congo rainforest. *Nat. Clim. Chang.* **9**, 617–622 (2019).
39. A. G. Konings, N. Holtzman, K. Rao, L. Xu, S. S. Saatchi, Interannual variations of vegetation optical depth are due to both water stress and biomass changes. *Geophys. Res. Lett.* **48**, e2021GL095267 (2021).
40. X. Xu *et al.*, Leaf surface water, not plant water stress, drives diurnal variation in tropical forest canopy water content. *New Phytol.* **231**, 122–136 (2021).
41. T. van Emmerik *et al.*, Water stress detection in the Amazon using radar. *Geophys. Res. Lett.* **44**, 6841–6849 (2017).
42. V. Leitold *et al.*, El Niño drought increased canopy turnover in Amazon forests. *New Phytol.* **219**, 959–971 (2018).
43. I. Aleixo *et al.*, Amazonian rainforest tree mortality driven by climate and functional traits. *Nat. Clim. Chang.* **9**, 384–388 (2019).
44. L. Xu *et al.*, Changes in global terrestrial live biomass over the 21st century. *Sci. Adv.* **7**, eabe9829 (2021).
45. W. Hubau *et al.*, Asynchronous carbon sink saturation in African and Amazonian tropical forests. *Nature* **579**, 80–87 (2020).
46. S. S. Saatchi *et al.*, Detecting vulnerability of humid tropical forests to multiple stressors. *One Earth* **4**, 988–1003 (2021).
47. A. Dai, Increasing drought under global warming in observations and models. *Nat. Clim. Chang.* **3**, 52–58 (2013).
48. B. W. Griscom *et al.*, Natural climate solutions. *Proc. Natl. Acad. Sci. U.S.A.* **114**, 11645–11650 (2017).
49. R. Crapolicchio *et al.*, ERS-2 scatterometer: Mission performances and current reprocessing achievements. *IEEE Trans. Geosci. Remote Sens.* **50**, 2427–2448 (2012).
50. J. Verbesselt *et al.*, Detecting trend and seasonal changes in satellite image time series. *Remote Sens. Environ.* **114**, 106–115 (2010).